Published in final edited form as:
Conf Proc IEEE Eng Med Biol Soc. 2014 August ; 2014: 5627–5630. doi:10.1109/EMBC.2014.6944903.

Estimation of Ultrasound Strain Indices in Carotid Plaque and Correlation to Cognitive Dysfunction

X Wang [IEEE Student Member],
University of Wisconsin-Madison, Madison, WI 53706 USA, phone: 608-772-8929; fax: 608-262-2413

D.C. Jackson,
University of Wisconsin-Madison, Madison, WI 53706 USA, phone: 608-772-8929; fax: 608-262-2413

C.C. Mitchell,
Department of Biomedical Sciences, University of Wisconsin-Milwaukee, Milwaukee, WI 53201 USA

T. Varghese [IEEE Senior Member],
University of Wisconsin-Madison, Madison, WI 53706 USA, phone: 608-772-8929; fax: 608-262-2413

B.P. Hermann,
University of Wisconsin-Madison, Madison, WI 53706 USA, phone: 608-772-8929; fax: 608-262-2413

M.A. Kliewer, and
University of Wisconsin-Madison, Madison, WI 53706 USA, phone: 608-772-8929; fax: 608-262-2413

R. J. Dempsey
University of Wisconsin-Madison, Madison, WI 53706 USA, phone: 608-772-8929; fax: 608-262-2413

X Wang: xwang235@wisc.edu

Abstract

Carotid plaque prone to release emboli may be predicted by increased strain variations within plaque due to arterial pulsation over a cardiac cycle. Non-invasive ultrasound strain imaging may therefore be a viable surrogate to determine the risk of embolic stroke and possible cognitive impairment. Ultrasound strain imaging was performed on 24 human subjects with significant plaque, who also underwent standardized cognitive assessment (Repeatable Battery for the Assessment of Neuropsychological Status (RBANS)) prior to a carotid endarterectomy (CEA) procedure. Radiofrequency signals were acquired using a Siemens Antares with a VFX 13-5 linear array transducer. Plaque regions were segmented by a radiologist at end-diastole using the Medical Imaging Interaction Toolkit. A hierarchical block-matching motion tracking algorithm was utilized to estimate the cumulated axial, lateral, and shear strains within the imaging plane. The maximum strain indices of the plaque, defined as mean accumulated strain over a small region of interest in the plaque with large deformations, were obtained. All the strain indices were

then correlated with RBANS Total score. Overall cognitive performance was negatively associated with maximum axial and lateral strains respectively. The results demonstrate a direct relationship between the maximum axial and lateral strain indices in carotid plaque and cognitive impairment.

I. Introduction

Micro-emboli that originate from rupture of carotid plaques may flow into the vasculature of the brain and may cause ischemic events resulting in stroke, vascular cognitive impairment or both [1]. Twice as many stroke patients may experience vascular cognitive impairment [2]. Studies have shown that cerebral micro-emboli correlate significantly with dementia and are associated with faster cognitive decline [3–4]. Silent strokes, without clinical symptoms, may occur in addition to clinically recognized stroke, and are actually five times more prevalent [5]. Studies have suggested that silent stroke may occur with concurrent subclinical emboli [6] and may cause accumulated cognitive decline [7].

Vulnerable plaque, defined as plaque capable of developing sudden clinically-significant thrombosis or embolization, undergoes significant deformation and thereby strain variations due to arterial pulsations during a cardiac cycle. Noninvasive ultrasound strain imaging [8] can be utilized to evaluate the mechanical deformation of plaque, and therefore may play an important role in the characterization of plaque vulnerability [9]. Maurice et al. [10] utilized a Lagrangian speckle model estimator to calculate the strain tensor and estimated axial, lateral, shear and radial strain in the plaque from the strain tensor. Schmitt et al. [11] implemented a model to calculate strain tensors on both transverse and longitudinal artery views. They found that the estimated axial and axial shear strain may characterize plaque composition and mechanical properties. Shi et al. [12] developed a multi-level tracking algorithm to accumulate displacement and strain in the carotid plaque, and showed that axial strain and lateral displacement can separate soft plaques from calcified ones. Ma et al. [13] demonstrated that Lagrangian strain estimation for short-axes view of the heart and on cross-sectional artery views shows better performance than an Eulerian approach for strain estimation. McCormick et al. [14] developed a Lagrangian strain estimation algorithm based on a hierarchical multi-level framework utilizing Bayesian regularization to estimate all components of the strain tensor, and found that the cumulated strain indices derived from the strain tensor are capable of quantifying vulnerability of carotid plaque.

In this work, we utilize the algorithms developed by our group [15] to further evaluate the distribution and variation of axial, lateral and shear strains for *in vivo* carotid plaque. We also focus on the correlation between cognitive function and multiple strain indices.

II. Data Acquisition

Ultrasound imaging was performed on 24 patients who presented with significant plaque, prior to a carotid endarterectomy procedure (CEA) at the University of Wisconsin-Madison Hospitals and Clinics. Patients provided informed consent using a protocol approved by the University of Wisconsin-Madison Institutional Review Board (IRB) before the ultrasound

and strain imaging study. The patients ranged from in age from 44 to 79 years, with a mean age of 65.88 ± 8.74.

Radiofrequency (RF) echo signals, along with clinical B-mode and color-flow Doppler images, were acquired using a Siemens Antares ultrasound system (Siemens Ultrasound, Mountain View, CA, USA) equipped with a VFX 13-5 linear transducer. The transmit frequency of the transducer was 11.4 MHz with a single transmit focus at the depth of plaque. The total depth of the B-mode image was 4 cm, with the lateral field width of 3.8 cm comprising 508 A-lines. At least two cardiac cycles of RF data were obtained and digitized at a sampling frequency of 40 MHz. Segmentation of plaque regions was performed on three end-diastolic frames by a radiologist using the Medical Imaging Interaction Toolkit (MITK) on the B-mode images reconstructed from RF data. Clinical B-mode and color-flow Doppler images acquired at the time of RF data acquisition were also used by the radiologist to better determine the plaque borders.

Clinical findings delineated 16 out of 24 patients as symptomatic and 7 as asymptomatic. One patient could not be classified. A patient was classified as symptomatic if he or she presented with stroke symptoms or a transient ischemic attack (TIA). Asymptomatic patients, on the other hand, were diagnosed with carotid stenosis without prior neurological clinical symptoms. All patients underwent objective cognitive assessment (Repeatable Battery for the Assessment of Neuropsychological Status (RBANS)) which provides an index of overall cognitive status (RBANS Total) as well as five indices reflecting specific cognitive abilities [16]. To reduce the number of comparisons only the RBANS Total score was used to correlate with the strain indices.

III. Strain Indices Estimation

Plaque strain assessment was conducted by an investigator blinded to the cognitive results. A block-matching motion tracking algorithm using a hierarchical framework developed in our laboratory [14] was utilized to estimate strain indices. Displacements between pre- and post-deformation frames were tracked with a three-level block-matching technique. The matching block was 15 × 28 pixels at the top level, and 10 × 18 pixels at the bottom level, with no overlap between the blocks. Along the axial direction a pixel represents 0.02 mm, while along the lateral direction a pixel represents 0.075 mm. Normalized cross-correlation analysis was performed using recursive Bayesian regularization over three iterations to improve the quality of the tracked displacements at each level for both axial and lateral displacements [17]. A dynamic frame skip method was utilized to obtain optimal motion tracking over a cardiac cycle, with a shorter frame skip during systole and a longer frame skip during end diastole. The threshold for frame skip was an absolute axial strain of 5% within a sub-region of the image. Incremental local displacements were then estimated in each frame and filtered with a 3 × 3 pixel median filter to remove outliers. Finally the local strain distribution was assessed by applying a modified least-squares fit over a 7-pixel length from displacement estimation accumulated over a cardiac cycle using the end-diastolic frame as the reference frame. Displacements and strains between consecutive frames calculated by the block-matching motion tracking algorithm were relatively small, due to the fact that the frame rates we used were no less than 27 fps. Therefore accumulated strain

indices over a cardiac cycle were presented to better characterize the elasticity of plaque tissue.

We utilized this method to estimate the accumulated axial, lateral, and shear strain distribution in the plaque regions identified within the imaging plane. Strain values were computed inside the segmented plaque and overlaid on the B-mode images. A typical axial strain image is shown in Fig. 1. The axial strain magnitude and direction are depicted on the color bar overlaid on the gray-scale B-mode images. Positive strain indicates tissue expanding or stretching, while negative strain denotes compression. Some high positive strain values can be found at the plaque-lumen interface and inside the plaque, suggesting that the plaque may stretch into the lumen during arterial pulsation. The corresponding lateral and shear strain images of the same plaque are shown in Fig. 2 and Fig. 3, respectively, with the same magnitude scale and color-coding for direction of strain. Similar to axial strain distributions, lateral strain is higher at the plaque boundary adjacent to or protruding into the blood flow than other areas. A more heterogeneous shear strain distribution in the plaque can be observed. Note that unlike axial and lateral strains, larger shear strains occur closer to the interface of plaque and vessel wall, where high axial or lateral strains do not necessarily exist.

IV. STRAIN INDICES AND COGNITION

A small region of interest (ROI) of 10–20 data points in the plaque with maximum strain was located on the strain image in each frame. The maximum strain in the plaque was then defined as the maximum of average strain value in this small ROI over two cardiac cycles to reduce noise. All strain indices were then correlated with RBANS Total scores using Pearson's correlation coefficients with a significance level of $p<0.05$ using a two-tailed *t*-test. A linear fit was performed for symptomatic, asymptomatic and for all patients respectively to show the correlation of strain and cognitive function in each group. All correlations and *p*-values are listed in Table 1. Significant correlations are labeled with an asterisk.

The maximum axial and lateral strains correlate significantly with cognition for the symptomatic group and for all patients with an *r* value around 0.5. No significant correlation with maximum shear strain is observed for any of the groups, and the correlations are much weaker for shear strain than axial and lateral strain indices. The RBANS Total score shows a negative correlation with the maximum strain indices. Note that the linear fits for the symptomatic group generally follow the trend of the entire group of patients. A decrease in the correlation with asymptomatic patients is also observed.

V. Discussion

In this study we demonstrate that a relationship exists between cognitive function and the maximum axial and lateral strain indices. Cognitive function for these patients declines with an increase in the axial and lateral strain indices in plaque. Since these strain indices primarily reveal the extent of deformation of plaque based on pulsatile flow in the carotid over the cardiac cycle, where larger deformations may indicate the presence of softer areas in plaques or variability in plaque composition over its length, higher strain values may

therefore suggest an increased probability of plaque rupture in these softer plaques. Deformation of the carotid wall and plaque is caused by a combination of wall shear stress, wall tensile stress and cyclic force induced by the pulsatile blood pressure [18–21]. The buildup of plaque disrupts blood flow and results in hemodynamic changes such as high velocity jets that introduce shear stresses and turbulence which lead to blood pressure fluctuations over the length of the blood vessel [22–24]. Re-circulating flow, high shear stresses and increasing turbulence in turn can accelerate plaque rupture [25–29]. As a consequence of plaque rupture, micro-emboli may flow into the brain and cause ischemic events leading to stroke and/or cognitive impairment. This study helps establish the relationship between increasing strain indices in carotid plaque and cognitive impairment through embolism.

Previous studies have shown that the noise artifacts are significantly higher for lateral strain estimation than in the axial direction due to the relatively small sizes of plaques compared to the lateral resolution of ultrasound image, as well as their heterogeneous nature [12]. Shear strain estimation may therefore induce more artifacts since it is neither aligned nor perpendicular to the ultrasound beam. Our improved Lagrangian algorithm enables better tracking of the lateral deformation and thereby more reliable lateral strain estimation [14]. The fact that lateral strain indices also show strong correlations with cognitive status indicates the robustness of the method, proving that this algorithm is able to characterize strain and therefore can be utilized to quantify vulnerability of carotid plaque.

Most plaques are heterogeneous and difficult to classify clinically as soft or calcified. However, the distribution of local strains within the plaque may reveal variations in plaque stiffness, which suggests that regions with higher strains may tend to break off and detach from the rest of plaque. High local strains can still occur in a plaque with lower mean strain values due to this heterogeneity. Therefore it is reasonable and appropriate to use maximum strain indices to quantify the vulnerability of plaque. This is consistent with our observation that maximum axial and lateral strains correlate significantly with cognitive impairment. From the shear strain distribution we hypothesize that the lack of significant correlations between cognition and maximum shear strain may be due to the fact that the highest shear strains are embedded deeper into the vessel wall instead of inside the plaque. Therefore sub-regional strain analysis near the vessel wall or at the wall-plaque interface may worth investigating in future work.

All patients in this study presented with over 50% stenosis and were therefore in need of CEA procedure [30], even for asymptomatic patients who had no prior stroke or TIA based on clinical findings. However these asymptomatic patients may have experienced silent stroke with subsequent cognitive dysfunction [7], which agrees with our observation that RBANS Total scores (83.43±7.41) of asymptomatic patients do not deviate from that of symptomatic patients (86.81±16.63). Studies have shown that the risk of silent stroke is positively related to the extent of carotid stenosis for both symptomatic and asymptomatic patients [31]. Additionally, we can observe possible fissures inside asymptomatic plaque from strain distributions. Therefore asymptomatic patients may still have great potential for developing emboli.

Replication with a larger sample of patients is required to further establish this relationship. The correlation not being significant for the asymptomatic group may be due to the smaller sample size. More correlations of strain indices to each of the RBANS component scales may also be enlightening.

VI. Conclusion

In summary, the results reveal a significant relationship between maximum axial and lateral strain indices in carotid plaque with cognitive function. Since strain indices estimated using this robust algorithm are capable of quantifying vulnerability of plaque, ultrasound strain imaging may assist in the identification of plaques prone to rupture, predicting embolism and preventing potential strokes.

Acknowledgments

This work was supported in part by NIH grants R21 EB010098-02, R01 NS064034-04, and 2R01 CA112192-06. This research was performed using the computational resources provided by the UW-Madison Center For High Throughput Computing (CHTC) in the Department of Computer Sciences. The CHTC is supported by UW-Madison and the Wisconsin Alumni Research Foundation, and is an active member of the Open Science Grid, which is supported by the National Science Foundation and the U.S. Department of Energy's Office of Science. The authors would like to thank Ms. Pamela Winne for coordinating the data acquisition on patients.

References

1. Whisnant JP, Basford JR, Bernstein EF, Cooper ES, Dyken ML, Easton JD, Little JR, Marler JR, Millikan CH, Petito CK, Price TR, Raichle ME, Robertson JT, Thiele B, Walker MD, Zimmerman aRA. Special report from the National Institute of Neurological Disorders and Stroke. Classification of cerebrovascular diseases III. Stroke. Apr.1990 21:637–76. [PubMed: 2326846]
2. Hachinski V, Iadecola C, Petersen RC, Breteler MM, Nyenhuis DL, Black SE, Powers WJ, DeCarli C, Merino JG, Kalaria RN, Vinters HV, Holtzman DM, Rosenberg GA, Wallin A, Dichgans M, Marler JR, Leblanc GG. National Institute of Neurological Disorders and Stroke-Canadian Stroke Network vascular cognitive impairment harmonization standards. Stroke. Sep.2006 37:2220–41. [PubMed: 16917086]
3. Purandare N, Voshaar RC, Hardicre J, Byrne J, McCollum C, Burns A. Cerebral emboli and depressive symptoms in dementia. Br J Psychiatry. Sep.2006 189:260–3. [PubMed: 16946362]
4. Purandare N, Voshaar RC, Morris J, Byrne JE, Wren J, Heller RF, McCollum CN, Burns A. Asymptomatic spontaneous cerebral emboli predict cognitive and functional decline in dementia. Biol Psychiatry. Aug 15.2007 62:339–44. [PubMed: 17531959]
5. Vermeer SE, Prins ND, den Heijer T, Hofman A, Koudstaal PJ, Breteler MM. Silent brain infarcts and the risk of dementia and cognitive decline. N Engl J Med. Mar 27.2003 348:1215–22. [PubMed: 12660385]
6. Dempsey RJ, Vemuganti R, Varghese T, Hermann BP. A review of carotid atherosclerosis and vascular cognitive decline: a new understanding of the keys to symptomology. Neurosurgery. Aug. 2010 67:484–93. discussion 493–4. [PubMed: 20644437]
7. Elias MF, Sullivan LM, D'Agostino RB, Elias PK, Beiser A, Au R, Seshadri S, DeCarli C, Wolf PA. Framingham stroke risk profile and lowered cognitive performance. Stroke. Feb.2004 35:404–9. [PubMed: 14726556]
8. Ophir J, Cespedes I, Ponnekanti H, Yazdi Y, Li X. Elastography: a quantitative method for imaging the elasticity of biological tissues. Ultrason Imaging. Apr.1991 13:111–34. [PubMed: 1858217]
9. Varghese T. Quasi-Static Ultrasound Elastography. Ultrasound Clin. Jul.2009 4:323–338. [PubMed: 20798841]

10. Maurice RL, Ohayon J, Fretigny Y, Bertrand M, Soulez G, Cloutier G. Noninvasive vascular elastography: theoretical framework. IEEE Trans Med Imaging. Feb.2004 23:164–80. [PubMed: 14964562]
11. Schmitt C, Soulez G, Maurice RL, Giroux MF, Cloutier G. Noninvasive vascular elastography: toward a complementary characterization tool of atherosclerosis in carotid arteries. Ultrasound Med Biol. Dec.2007 33:1841–58. [PubMed: 17698283]
12. Shi H, Mitchell CC, McCormick M, Kliewer MA, Dempsey RJ, Varghese T. Preliminary in vivo atherosclerotic carotid plaque characterization using the accumulated axial strain and relative lateral shift strain indices. Phys Med Biol. Nov 21.2008 53:6377–94. [PubMed: 18941278]
13. Ma C, Varghese T. Lagrangian displacement tracking using a polar grid between endocardial and epicardial contours for cardiac strain imaging. Med Phys. Apr.2012 39:1779–92. [PubMed: 22482601]
14. McCormick M, Varghese T, Wang X, Mitchell C, Kliewer MA, Dempsey RJ. Methods for robust in vivo strain estimation in the carotid artery. Phys Med Biol. Nov 21.2012 57:7329–53. [PubMed: 23079725]
15. Wang X, Jackson DC, Varghese T, Mitchell CC, Hermann BP, Kliewer MA, Dempsey RJ. Correlation of cognitive function with ultrasound strain indices in carotid plaque. Ultrasound Med Biol. Jan.2014 40:78–89. [PubMed: 24120415]
16. Randolph C, Tierney MC, Mohr E, Chase TN. The Repeatable Battery for the Assessment of Neuropsychological Status (RBANS): preliminary clinical validity. J Clin Exp Neuropsychol. Jun. 1998 20:310–9. [PubMed: 9845158]
17. McCormick M, Rubert N, Varghese T. Bayesian regularization applied to ultrasound strain imaging. IEEE Trans Biomed Eng. Jun.2011 58:1612–20. [PubMed: 21245002]
18. Lee RT. Atherosclerotic lesion mechanics versus biology. Z Kardiol. 2000; 89(Suppl 2):80–4. [PubMed: 10769408]
19. Gao H, Long Q. Effects of varied lipid core volume and fibrous cap thickness on stress distribution in carotid arterial plaques. J Biomech. Oct 20.2008 41:3053–9. [PubMed: 18786671]
20. Richardson PD, Davies MJ, Born GV. Influence of plaque configuration and stress distribution on fissuring of coronary atherosclerotic plaques. Lancet. Oct 21.1989 2:941–4. [PubMed: 2571862]
21. van der Wal AC, Becker AE. Atherosclerotic plaque rupture--pathologic basis of plaque stability and instability. Cardiovasc Res. Feb.1999 41:334–44. [PubMed: 10341833]
22. Kefayati S, Poepping TL. Transitional flow analysis in the carotid artery bifurcation by proper orthogonal decomposition and particle image velocimetry. Med Eng Phys. Jul.2013 35:898–909. [PubMed: 23025907]
23. Slager CJ, Wentzel JJ, Gijsen FJ, Schuurbiers JC, van der Wal AC, van der Steen AF, Serruys PW. The role of shear stress in the generation of rupture-prone vulnerable plaques. Nat Clin Pract Cardiovasc Med. Aug.2005 2:401–7. [PubMed: 16119702]
24. DePaola N, Gimbrone MA Jr, Davies PF, Dewey CF Jr. Vascular endothelium responds to fluid shear stress gradients. Arterioscler Thromb. Nov.1992 12:1254–7. [PubMed: 1420084]
25. Bluestein D, Niu L, Schoephoerster RT, Dewanjee MK. Fluid mechanics of arterial stenosis: relationship to the development of mural thrombus. Ann Biomed Eng. Mar-Apr;1997 25:344–56. [PubMed: 9084839]
26. Poepping TL, Rankin RN, Holdsworth DW. Flow patterns in carotid bifurcation models using pulsed Doppler ultrasound: effect of concentric vs. eccentric stenosis on turbulence and recirculation. Ultrasound Med Biol. Jul.2010 36:1125–34. [PubMed: 20447759]
27. Stein PD, Sabbah HN. Measured turbulence and its effect on thrombus formation. Circ Res. Oct. 1974 35:608–14. [PubMed: 4278187]
28. Loree HM, Kamm RD, Atkinson CM, Lee RT. Turbulent pressure fluctuations on surface of model vascular stenoses. Am J Physiol. Sep.1991 261:H644–50. [PubMed: 1887914]
29. Reininger AJ, Reininger CB, Heinzmann U, Wurzinger LJ. Residence time in niches of stagnant flow determines fibrin clot formation in an arterial branching model--detailed flow analysis and experimental results. Thromb Haemost. Sep.1995 74:916–22. [PubMed: 8571321]
30. Hanley D, Gorelick PB, Elliott WJ, Broder MS, Saver JL, Kidwell CS, Fagan SC, Wilson A, Lennihan L, Schwer WA, Rubenstein LZ, Crowell RM, Haines SJ, Lopez CC, Zorowitz R, Dubois

RW. Determining the appropriateness of selected surgical and medical management options in recurrent stroke prevention: a guideline for primary care physicians from the National Stroke Association work group on recurrent stroke prevention. J Stroke Cerebrovasc Dis. Sep-Oct;2004 13:196–207. [PubMed: 17903976]

31. Norris JW, Zhu CZ. Silent stroke and carotid stenosis. Stroke. Apr.1992 23:483–5. [PubMed: 1561676]

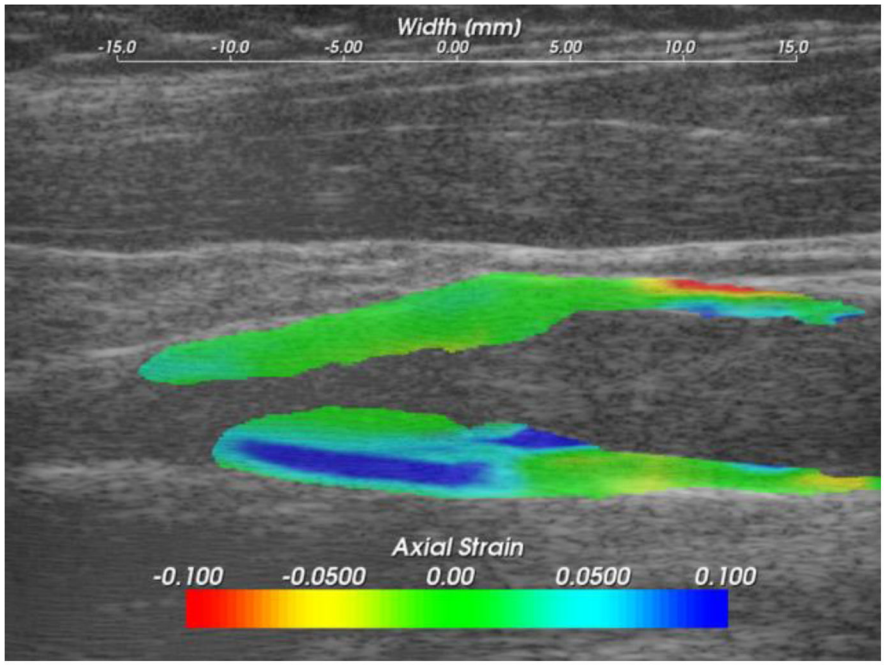

Figure 1.
Axial strain values overlaid on B-mode images.

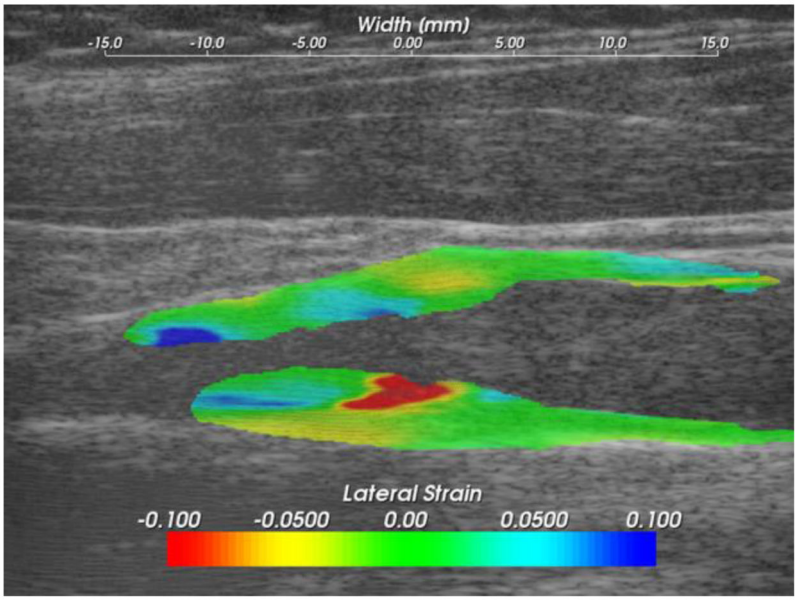

Figure 2.
Lateral strain values overlaid on B-mode images.

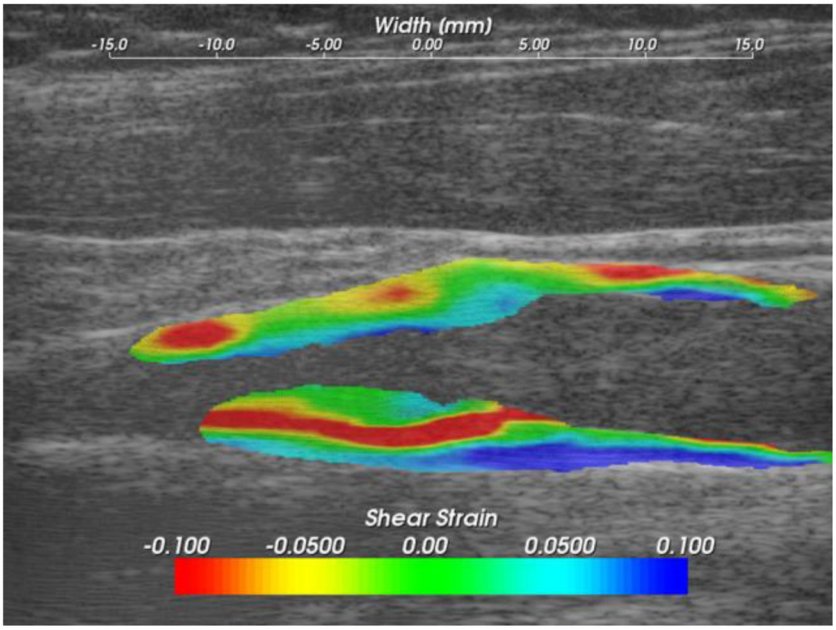

Figure 3.
Shear strain values overlaid on B-mode images.

TABLE I

Pearson's Correlation Coefficients and Significance Values

	Correlations of RBANS Total Score to Maximum Strain Indices		
	Axial	***Lateral***	***Shear***
Symptomatic	r=−0.533, p=0.032*[a]	r=−0.650, p=0.006*	r=−0.432, p=0.092
Asymptomatic	r=−0.530, p=0.205	r=−0.115, p=0.803	r=0.037, p=0.937
All	r=−0.491, p=0.014*	r=−0.501, p=0.012*	r=−0.345, p=0.097

[a] Significant correlations are labeled with *.